© 2017 IJSRSET | Volume 3 | Issue 1 | Print ISSN: 2395-1990 | Online ISSN : 2394-4099
Themed Section: Engineering and Technology

Sensitivity of WRF Model Output to Planetary Boundary Layer Height Variation over North Africa

Mostafa M. Ibrahim*[1], Mahmoud F. Abdel-Sattar[2]

[1,2]Department of Astronomy and Meteorology, Al-Azhar University, Cairo, Egypt

ABSTRACT

The first intention of this work was the modification of the Planetary Boundary Layer (PBL) Yonsei University scheme (YSU) in order to improve the estimation of Planetary Boundary Layer Height (PBLH) over Sahara desert during daytime. It is anticipated that the problem concerns the estimation of surface layer temperature. The surface boundary layer temperature, in the Revised YSU version (RYSU), is increased by (TSK-TT)/d when the skin temperature TSK > TT. It is found that when the parameter TT is 40o C the optimal value of the parameter d is around 3.5. Evaluation of WRF model forecast output when implemented with RYSU shows better performance for PBL atmospheric variables. The other intention of this work is to study the impact of using the WRF model implemented with RYSU scheme relative to that using YSU scheme. It is shown that the difference between the two models run is significant even far from the Sahara desert where the modification is applied. It is found that very small fast disturbances propagating out of a dipole vortex where the surface boundary layer temperature is modified excite specific locations forming local dipole vorticies. Out of these dipole vortices gravity waves propagate. Development that cause significant local variation in weather elements occur where the interaction evolve. It is found that deep convection areas are one of the possible specific locations where interaction can arises. One can argue that since very small propagating disturbances are part of our chaotic atmosphere, the side effect that resembles the Butterfly effect could be numerical rather than physical outcome.

Keywords : PBL height, WRF Model, YSU Scheme, Weather Forecast

I. INTRODUCTION

Accurate modeling of Planetary Boundary Layer (PBL) processes is essential for forecasting weather and climate (Garcia-Menendez et al. 2013). One of the most important variables that are essential for accurate PBL simulation for mesoscale and climate models is the Planetary Boundary Layer Height (PBLH). This variable that delineates the top of the atmospheric mixing layer is a key to understand and estimate vertical transport processes that occurs between PBL and the free atmosphere. It is also a basic parameter in air quality control and pollutant dispersion (Bao et al. 2008; Cheng et al. 2012; Gilliam et al. 2012; Garcia-Diez et al. 2013). Unfortunately, this variable is not routinely measured nor does it have a standard universal definition. As a result, there are differences that may be significant between model results in estimating this variable. There are several methods to estimate this parameter using atmospheric variables such as the vertical profile of potential temperature, relative humidity, specific humidity, wind speed, and atmospheric refractivity (Sugiyama and Nasstrom 1999). Also evaluation of PBLH can be done using the well-known dimensionless Richardson number Ri (Richardson et al. 2013; Zhang et al. 2014). This parameter that is obtained from the dimensionless turbulent kinetic energy equation, represents the ratio between buoyancy production or consumption term and the mechanical or shear production term. One definition of PBL depth is that layer where turbulent mixing occurs due to the presence of ground; one can specify PBLH as that depth where Ri exceeds some critical value.

Ao et al. (2012) use Global Positioning System Radio Occultation (GPSRO) measurements to derive a global climatology of PBLH. Their paper indicates that the highest PBLH occurs over desert areas in summer months. The paper shows that the estimated monthly summer average (JJA) of PBLH in the Sahara Desert region (20_N to 30_N; 0_E to 15_E), exceeds 3 km in the afternoon. Besides Banks et al. (2015) use the lidar extended Kalman filter to estimate PBLH over Barcelona, Spain for 45 individual days during a seven year period. The overall conclusion is systematic underestimation of PBLH in the WRF model. Experiments, not shown, using WRF NWP model with different PBL schemes indicate lower values over the Sahara Desert than anticipated by Ao et al. (2012) for summer cases with clear skies. One can anticipate that there is a large correlation between high PBLH and skin temperature. Since skin temperature differs from the traditional 2-meter air surface temperature in its physical meaning, magnitude, and measuring technique (Jin and Dickinson 2010), one can expect that both variables are necessary for good PBL simulation. This is crucial when the magnitude difference between the two variables become large. This is the case over desert areas on summer clear days where the difference can exceed 15o C (Jin and Dickinson 2010). In this paper we will force an increase of PBLH over North Africa Sahara Desert when the skin temperature reaches critical value then discuss the impact on the model output. The Yonsei University (YSU) PBL scheme (Hong et al. 2006) is chosen since experiments indicate better simulation over North Africa relative to other PBL schemes (Ibrahim et al. 2012).

II. DATA AND METHODOLOGY

In this study, the impact of modifying the PBL YSU scheme on the output of WRF model forecast is investigated. WRF model version 3.6.1 is used to forecast eighteen days during June, July and August of 2003 (six days each month). The model domain in the x, y and z coordinates has $113 \times 72 \times 34$ grid points with a $54\,km$ horizontal grid resolution ($5^{\circ}N$ to $40^{\circ}N$; $15^{\circ}W$ to $45^{\circ}E$). The top model level is at $50\,mb$ $(\approx 20\,km)$, and the model integrated time step is 300 seconds. The physical parameterization schemes used in the present work include the rapid radiative transfer model (RRTM) for long wave, Duhia scheme for shortwave radiation, Grill-Freitas ensemble convective scheme, and the Noah land surface scheme. It is aimed to force an increase of PBLH over North Africa's Sahara Desert to simulate observations. The first order, nonlocal closure YSU scheme, (Hong et al. 2006) uses the following equation to estimate h (PBLH):

$$h = Rib_{cr}\frac{\theta_{va}\,|U(h)|^2}{g[\theta_v(h)-\theta_s]}, \quad (1)$$

where Rib_{cr} is the critical bulk Richardson number, U(h) is the horizontal wind speed at h, θ_{va} is the virtual potential temperature at the lowest model level, $\theta_v\ (h)$ is the virtual potential temperature at h, and θ_s is the appropriate temperature near the surface. θ_s that is expected to represents surface layer temperature is defined in YSU scheme as:

$$\theta_s = \theta_{va} + \theta_T, \quad (2)$$

where

$$\theta_T = b\frac{\overline{(w'\theta')}_0}{w_s}. \quad (3)$$

θ_T is the virtual temperature excess near the surface, w_s is the mixed-layer velocity scale, $\overline{(w'\theta')}_0$ is the virtual heat flux from the surface, and b is constant taken 7.8. Since θ_T is required to modify θ_s toward representing surface layer temperature, in this work an extra term $[(TSK-TT)/d]$ is added whenever $TSK > TT$, i.e (2) becomes:

$$\theta_s = \theta_{va} + \theta_T + (TSK-TT)/d, \quad (4)$$

where TSK is the skin temperature. As mentioned in the above section, the difference between skin and surface air temperatures can exceed $15^{\circ}C$ over the Sahara Desert on summer clear days. Estimation of θ_T when $w_s = 1\,m/s$ gives values less than $3.5^{\circ}C$ during the three forecast days. Also it is found that maximum values occur south of the Sahara Desert (around latitude $15^{\circ}N$). One expects in the case of large difference between skin and the model lowest level temperatures that the YSU scheme significantly underestimates the surface layer temperature. In addition increasing the value of b is not the appropriate solution. It is found that when TSK temperature is $40^{\circ}C$, the surface air

temperature is about $7^{\circ}C$ lower. In this work, TT is set as $40^{\circ}C$ aiming at better estimation of surface layer temperature. In other words whenever skin temperature exceeds $40^{\circ}C$, an extra term is added to θ_T . Experiments to obtain the optimal value of d are performed.

III. RESULTS AND DISCUSSION

In the following four data sets are compared. The ECMWF ERA-Interim reanalysis data with $0.5^{\circ} X 0.5^{\circ}$ grid size and three hours output time resolutions. The second data set is NCEP with space and time output resolution $0.5^{\circ} X 0.5^{\circ}$ and six hours respectively. These data sets are referred to as References Data (Rd_1 and Rd_2 respectively). The other two data sets are the forecast WRF model output with YSU scheme not modified MOD_1 and with modified YSU scheme MOD_2. The main reference data used in this work is Rd_1 since its time resolution is three hours.

ERA-Interim re-analysis data (Dee et al. 2011), is the output of the global ECMWF forecast model Cy31r1 with resolution T255 (triangular truncation at 255), N128 (128 latitude circles), L60 (60 model levels), and about 20 model levels in the lower layer ($0 \; to \; 5 \; km$). The traditional observed data such as surface weather observations and radiosonds are combined in an optimal way with Satellite observations from geostationary orbit (Meteosat, GOES, GMS), and from low earth orbit Satellites (NOAA, and DMSP). Furthermore, data from hyperspectral sounders such as IASI, AIRS, and radio occultation instruments such as CHAMP, COSMIC, and GRAS are assimilated. In several respects Rd_1 is found to be one of the best sources of global meteorological data. For example, von Engeln and Teixeira (2013) show that PBLH climatology generated from ERA-Interim re-analysis data captures many of the expected climatological features.

A. Optimal value of *d* in (4)

To obtain the optimal value of d when TT is set to be $40^{\circ}C$, the WRF model runs to forecast eighteen days during June, July, and August of 2003 (six days each month). Each situation is being forecasted nine times ($d = 1, 2, 3, 3.5, 4, 4.5, 5, 6,$ and infinity). The case with d equals infinity corresponds to the YSU scheme not modified.

Figure 1 displays the domain of study area average of PBLH error (Model forecast Rd_1) as function of d and the eighteen case studies. Each case study is 12 hours forecast error valid at $12 \; GMT$. Figure 2 is similar to Fig. 1 but for the root mean square error of PBLH. On the other hand, Fig. 3 demonstrates the mean of the eighteen case studies for the average error and the root mean square error of PBLH as function of d. The figures indicate that the minimum average error occurs between $d = 2$ and $d = 3$ while minimum root square error occurs around $d = 3.5$. It is also found that if the error is averaged only over the Sahara Desert (not over the whole domain of study) both the average and root mean square errors shift toward larger value of d. Since root mean square error is more representative of actual error than average error, in this work the value of d is taken to be 3.5. Allowing TT to change in order to obtain the optimal values of d and TT with larger sample of synoptic situations is not intended in this work. In the following three days forecast fields of the situation 20 July 2003 using MOD_1 and MOD_2, when $d = 3.5$, are compared with Rd_1 and Rd_2.

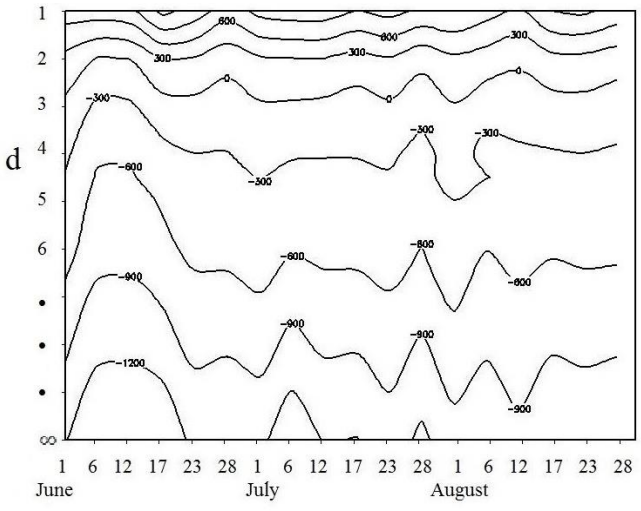

Figure 1. Area average over the domain of study for PBLH error (m) as function of the eighteen case studies and d.

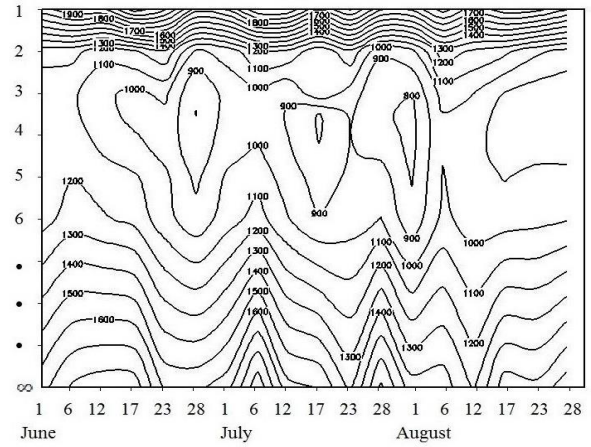

Figure 2. Same as Fig. 1 but for Root mean square PBLH error (m).

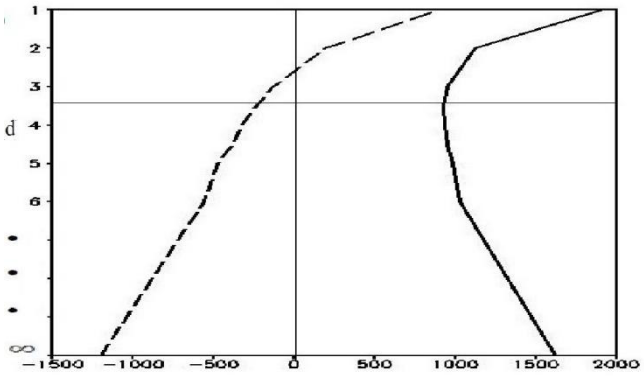

Figure 3. The average of the eighteen case studies for Figs. 1 and 2 (dashed and solid lines respectively).

B. PBLH forecast

Figure 4a,b,c display PBLH contour heights 3000, 4000, and 5000 meters for the four data sets Rd_1, Rd_2, MOD_1, and MOD_2 at 1200 GMT on 20, 21, and 22 July 2003 respectively. As expected MOD_2 has higher PBLH over the Sahara Desert than MOD_1. One also notes that MOD_2 is closer to the reference data Rd_1 and Rd_2 compared to MOD_1. Figure 5 shows mean PBLH over the area $``0^{\circ}E$ to $30^{\circ}E$; $20^{\circ}N$ to $30^{\circ}N"$ over Sahara Desert as a function of time. One can note that MOD_2 resemble the reference data Rd_1 and Rd_2 compared with MOD_1. From here on MOD_1, and MOD_2 will be compared only with Rd_1 (ECMWF reanalysis data) since it is available each three hours. The difference $(MOD\_2 - MOD\_1)$ of PBLH as function of latitude and time is displayed in Fig. 6. The figure shows mean PBLH for longitudes $5^{\circ}W$ to $30^{\circ}E$ as function of latitude and time. Large positive difference of PBLH over Sahara $(:15^{\circ}N$ to $:35^{\circ}N)$ is clear during daytime. One also note during late afternoon, unexpected narrow negative band where PBLH of MOD_1 is larger than that of MOD_2. This feature can be seen clearly in Fig. 7. Figure 7 displays $(MOD\_2 - MOD\_1)$ PBLH difference for the grid point $25^{\circ}N$; $2^{\circ}E$ as function of time. The figures show that there are negative areas, where PBLH of MOD_1 exceeds significantly that of MOD_2. These areas are of small scale type. The reason for this feature is discussed in the next section. In summary the modification done to YSU scheme achieves the required goal of modifying PBLH toward simulating PBLH observations over the Sahara Desert.

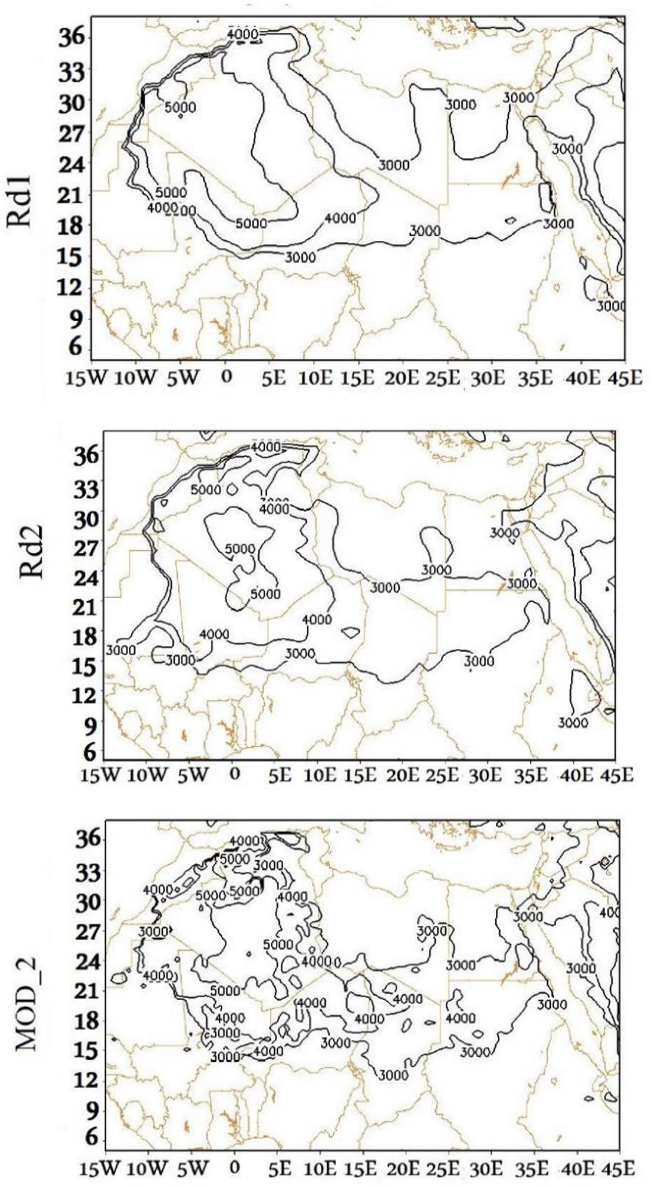

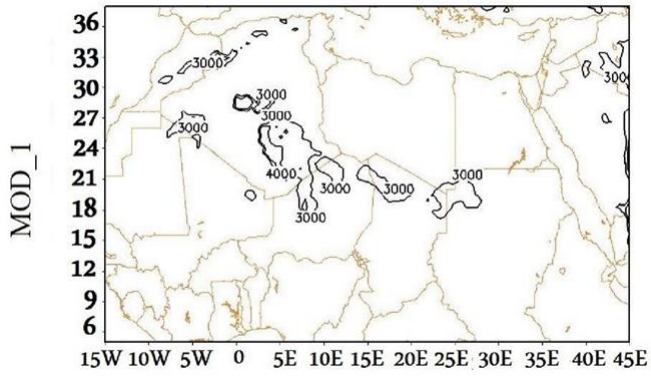

Figure 4a. PBLH $^{>4000}$ meters at 1200 GMT on 20 July 2003 from $^{MOD\_1}$, $^{MOD\_2}$, Rd_1 and Rd_2.
Figure 4b: same as Fig. 4a but on 21 July 2003.

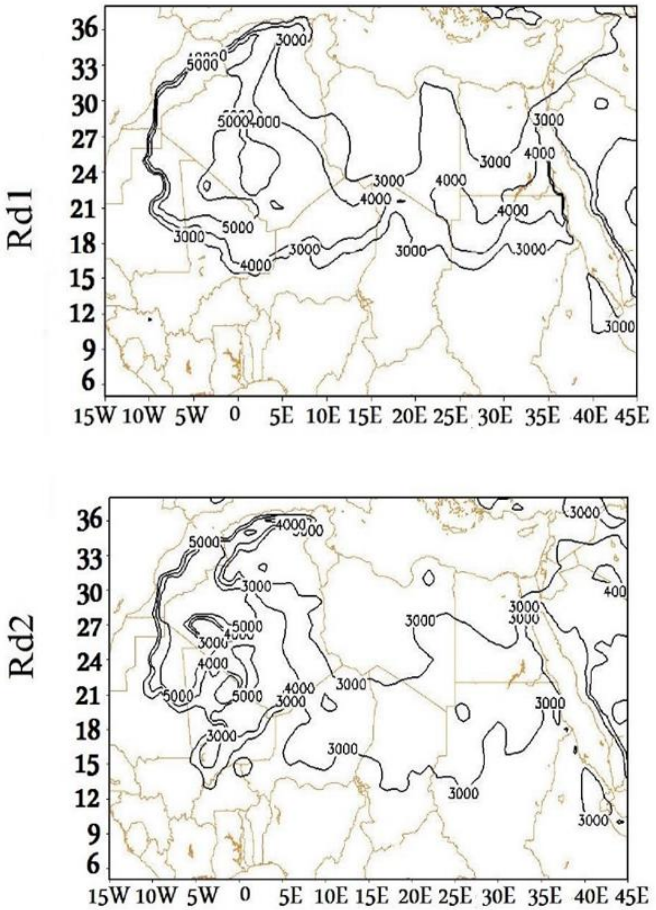

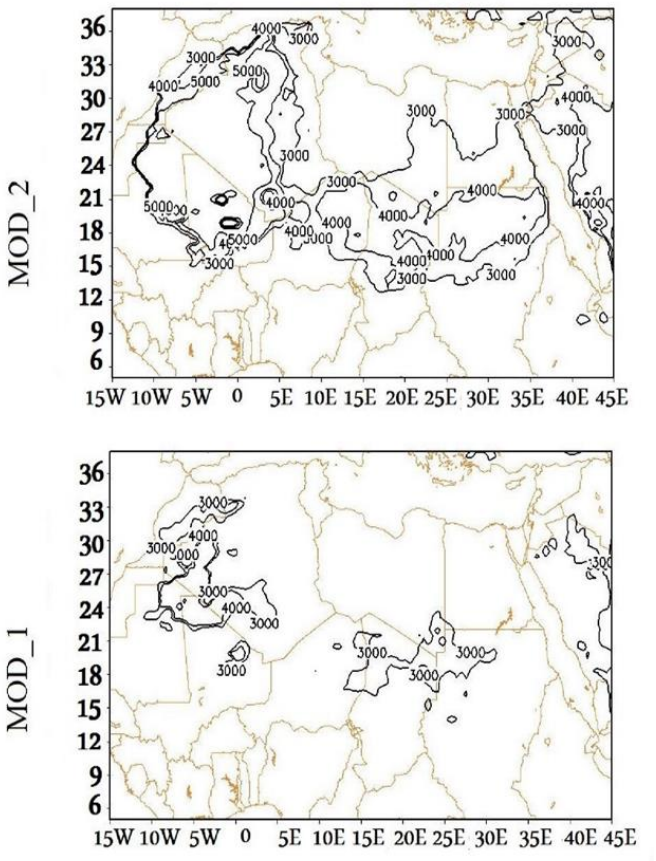

Figure 4b. Same as Fig. 4a but on 21 July 2003.

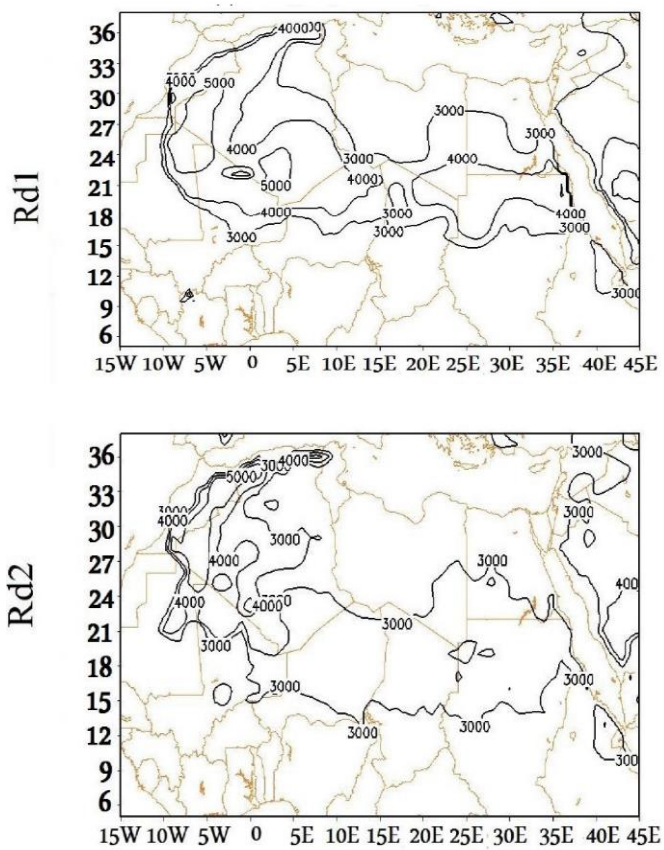

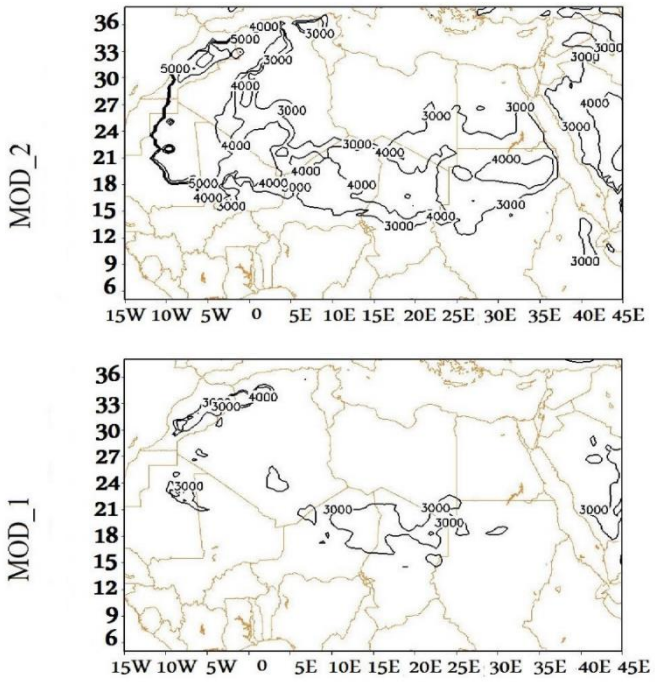

Figure 4c. Same as Fig. 4a but on 22 July 2003.

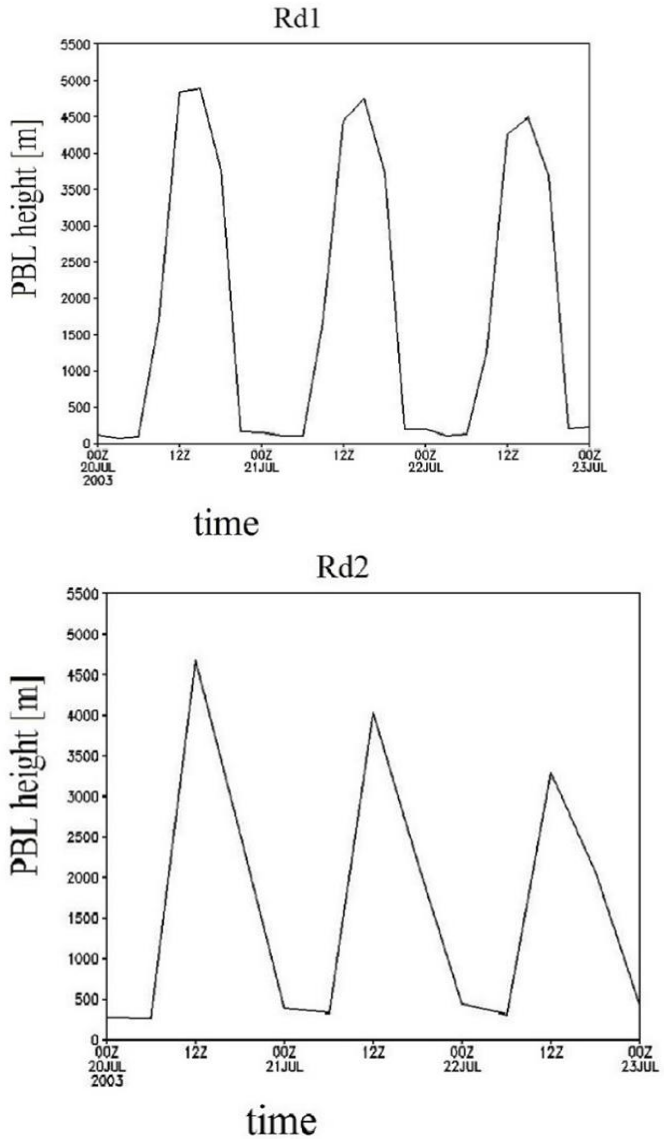

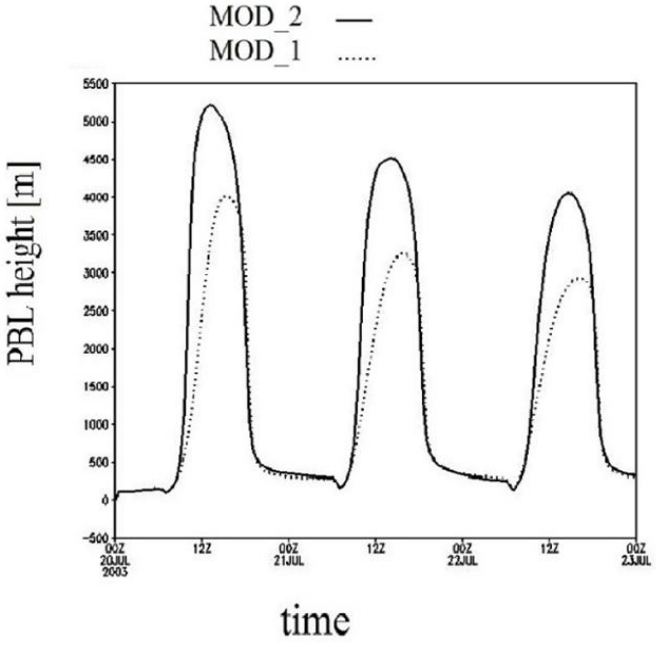

Figure 5. Mean PBLH over area on Sahara Desert ($00^{\circ}E$ to $30^{\circ}E; 20^{\circ}N$ to $30^{\circ}N$) versus model integrated time for MOD_1 , MOD_2, Rd_1 and Rd_2

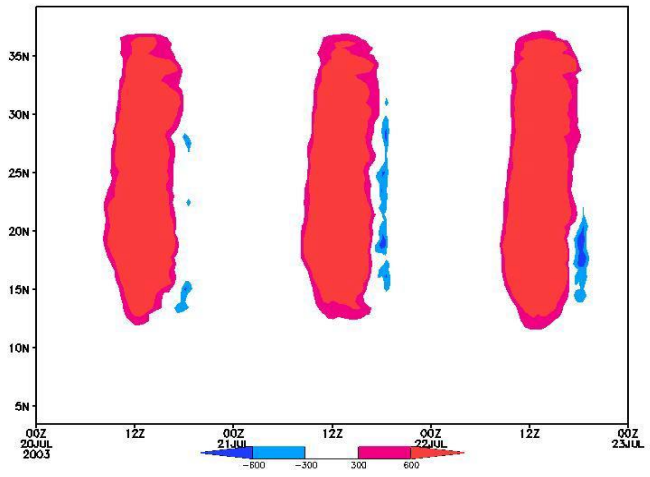

Figure 6. Average $(MOD\_2 - MOD\_1)$ PBLH (m) for the longitudes $5^{\circ}W$ to $30^{\circ}E$ as function of latitude and time.

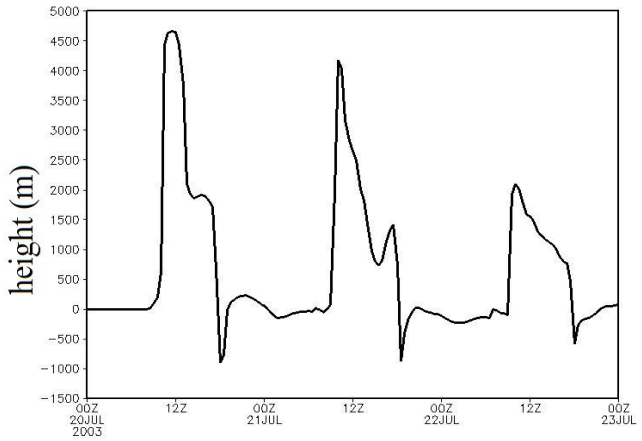

Figure 7. PBLH difference $(MOD\_2 - MOD\_1)$ for the grid point $25^{\circ}N$; $2^{\circ}E$ versus time.

C. Other forecast fields

Figure 8 shows vertical cross section of mean potential temperature difference $(MOD\_2 - MOD\_1)$ for longitudes $5^{\circ}W$ to $30^{\circ}E$ as function of latitude at 15 GMT on 20, 21 and 22 July 2003. Figure 9 is similar to Fig. 8 but for water vapor mixing ratio. Figures 8 and 9 indicate that, during daytime, over the Sahara Desert $(:15^{\circ}N$ to $:30^{\circ}N)$ there is higher values of temperature (water vapor mixing ratio) in the PBL (layer above PBL) for MOD_2 compared with MOD_1. In fact this feature is almost persisting during the forecast period as shown in Fig. 7. Figure 10 and 11 is similar to Fig. 8 and 9 respectively but only for latitudes $20^{\circ}N$ (lower) and $25^{\circ}N$ (upper) as function of time. The figures indicate that potential temperature (water vapor mixing ratio) for MOD_2 is higher (lower) than that of MOD_1 in PBL (layer above PBL). This indicates that MOD_2 has larger static instability compared with MOD_1 and has higher probability for cloud formation. Figure 12 is similar to Fig. 8 but for vertical distribution of forecasted cloud amount difference $(MOD\_2 - MOD\_1)$. More clouds in MOD_2 which is clear in Fig. 12 is expected to reduce the received surface energy during the daytime, and thus reducing the upward sensible heat flux that is used in estimating θ_T by (3). One should note that Fig. 12 gives the average cloud fraction difference $(MOD\_2 - MOD\_1)$ between longitudes $5^{\circ}W$ to $30^{\circ}E$ over the desert area where clouds are sparse. The small cloud fraction value 0.1 shown in Fig. 12 is indication of moisture accumulation above PBL (see also Figs. 8 and 11).

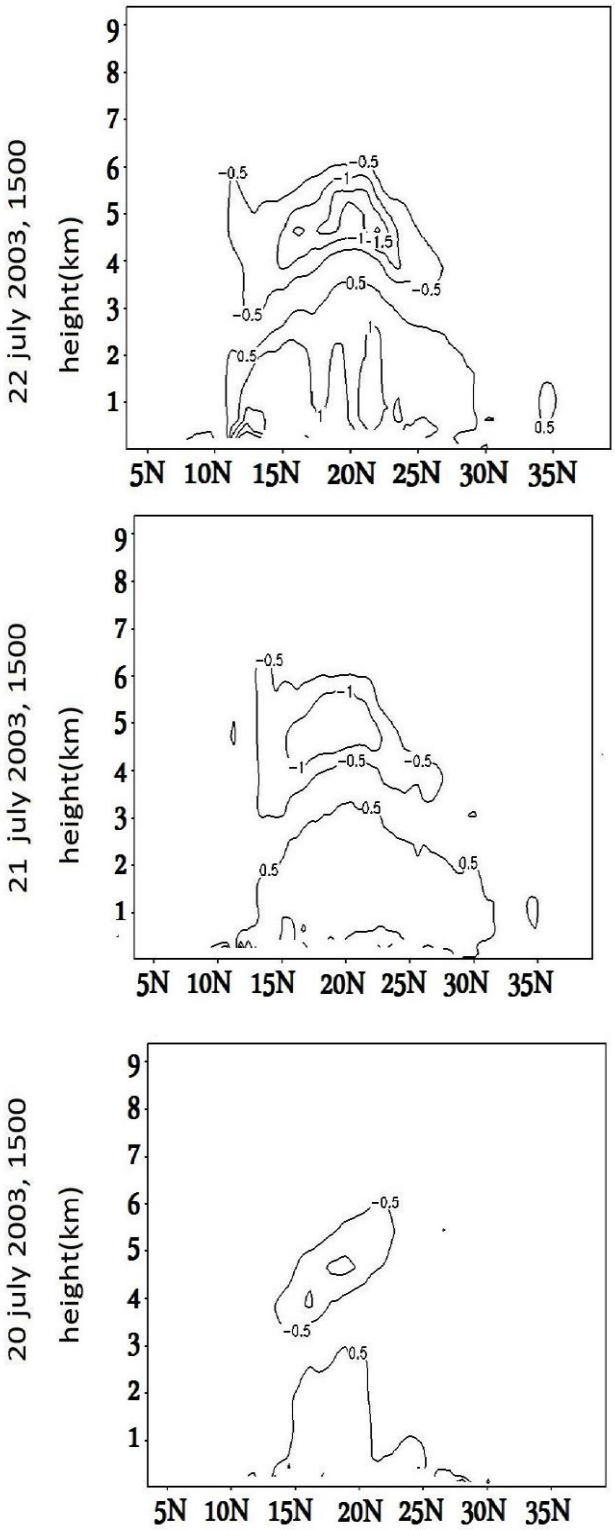

Figure 8. vertical cross section versus latitude for mean $(5^{\circ}W$ to $30^{\circ}E)$ potential temperature difference of $(MOD\_2 - MOD\_1)$

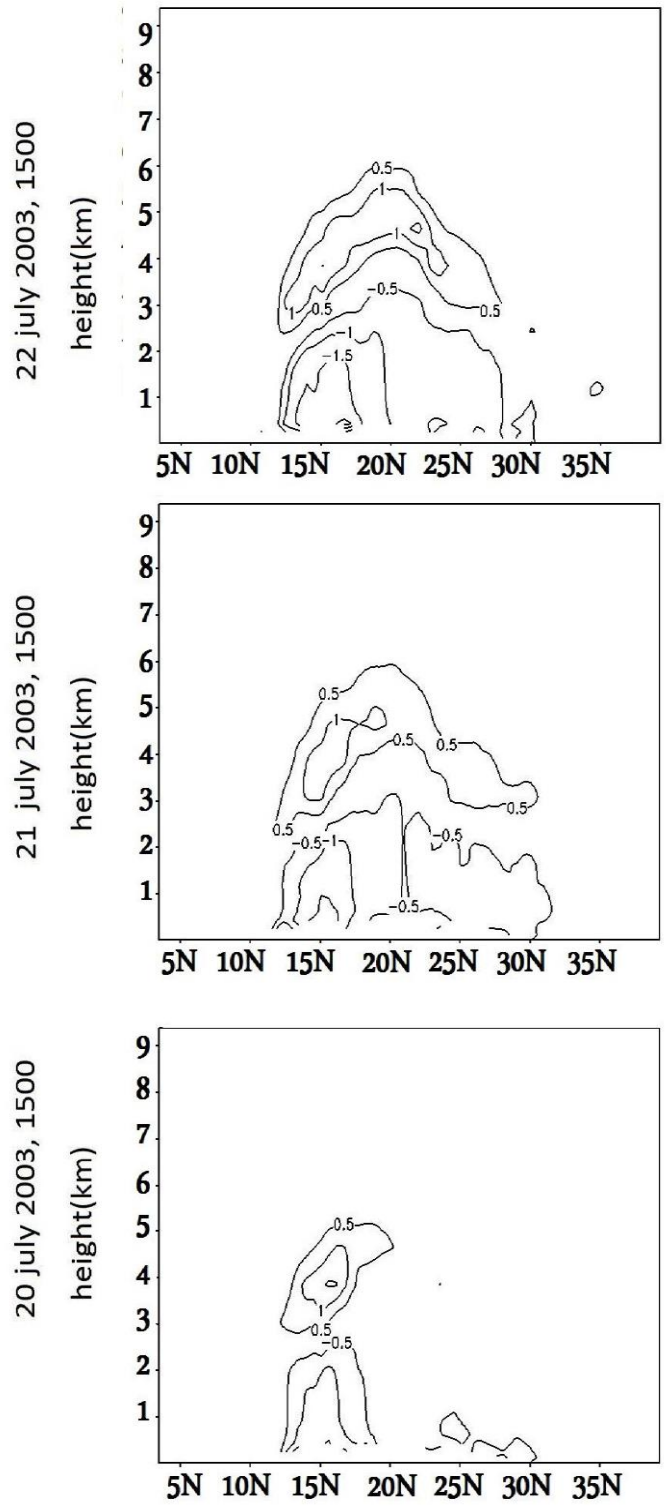

Figure 9. same as Fig. 8 but for water vapor mixing ratio difference $(MOD\_2 - MOD\_1)$.

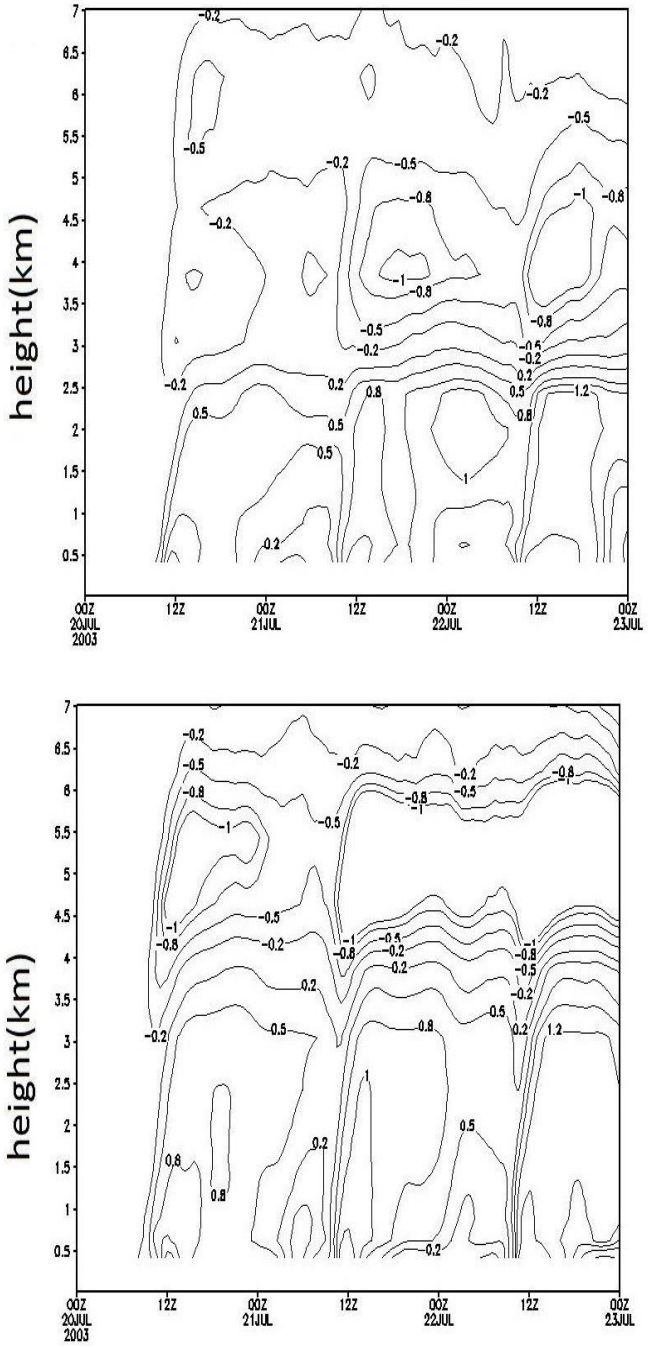

Figure 10. Vertical-time cross section of mean $(5^{\circ}W$ to $30^{\circ}E)$ at $25^{\circ}N$ (upper) $20^{\circ}N$ (lower) for potential temperature difference $(MOD\_2 - MOD\_1)$.

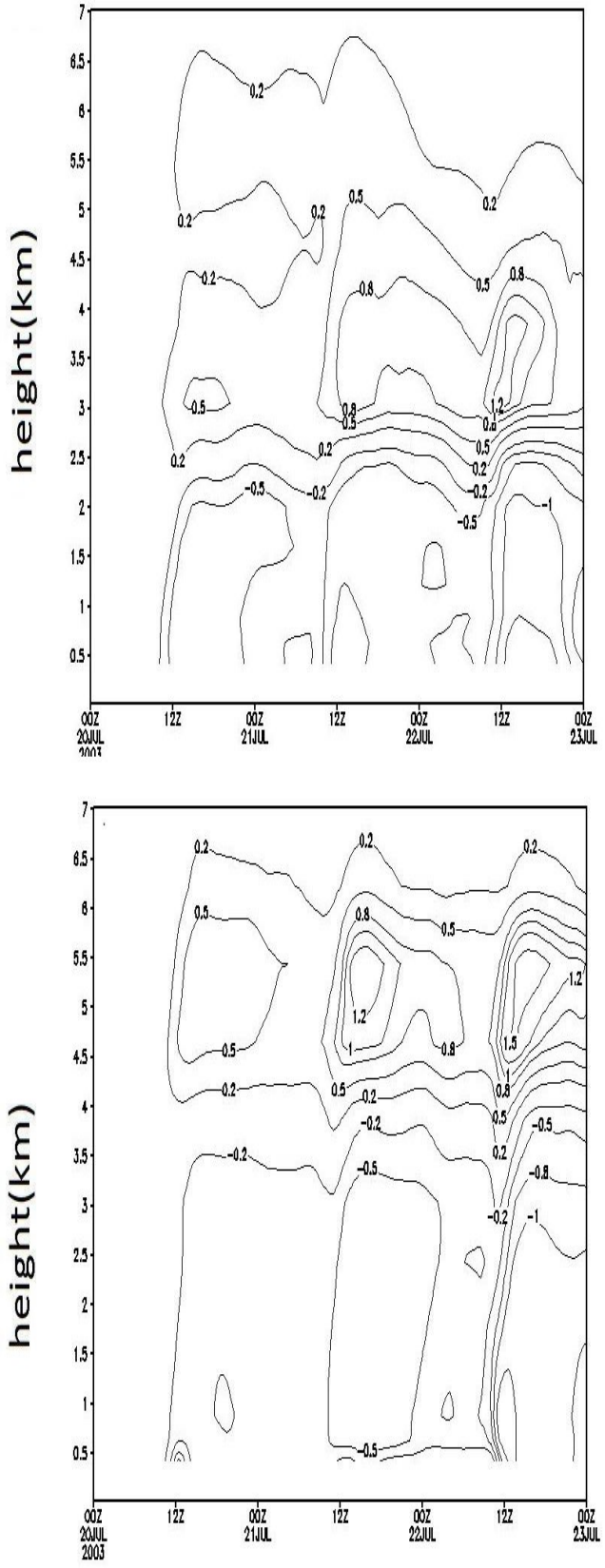

Figure 11. same as Fig. 10 but for water vapor mixing ratio difference $(MOD\_2 - MOD\_1)$.

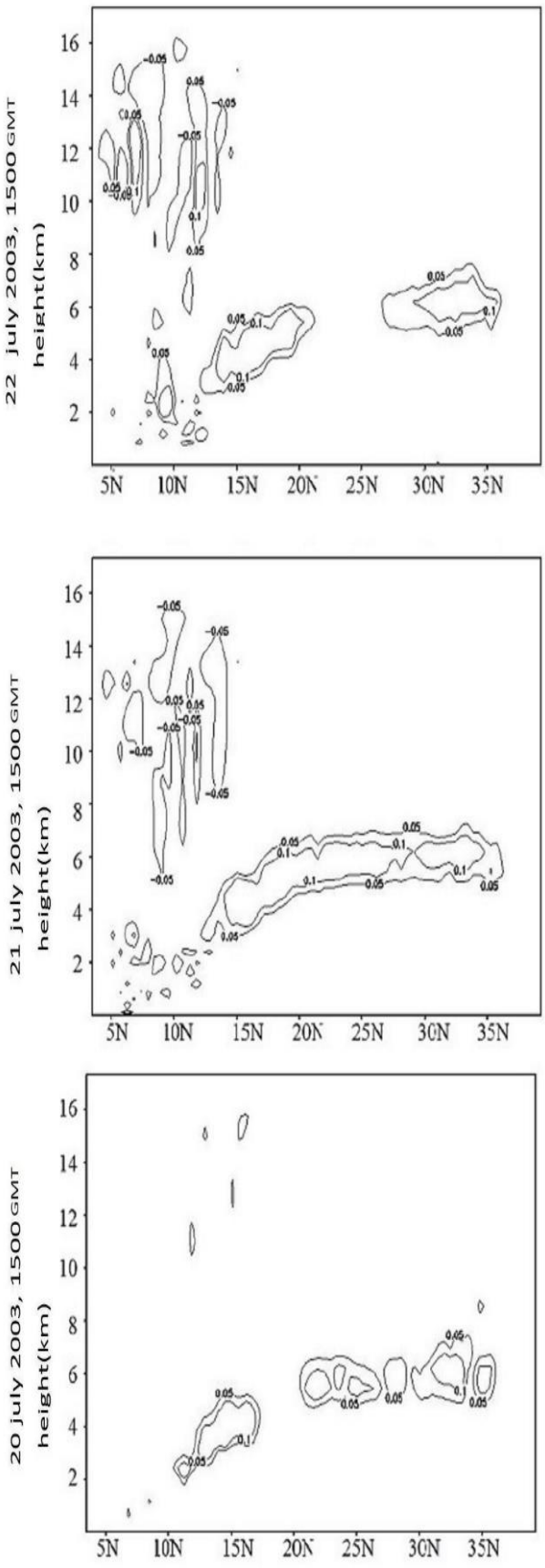

Figure 12. Same as Fig. 8 but for cloud fraction difference $(MOD\_2 - MOD\_1)$.

Figure 13 displays the average models difference $(MOD\_2 - MOD\_1)$ of the upward surface heat flux in W/m^2. One can argue that the existence of the narrow band where PBLH of MOD_1 exceeds that of MOD_2 is the byproduct of the decrease in surface upward sensible heat flux that is used in (3) to estimate PBLH by (1). It should be mentioned that (1) and (3) imply that there are other factors affecting PBLH. One of these factors is the horizontal wind speed at the top of PBL. Figure 10a which is similar to Fig. 8 but for horizontal wind speed difference $(MOD\_2 - MOD\_1)$. Figure 14 displays PBLH for both MOD_1 and MOD_2. The figure indicates that MOD_2 has less horizontal wind speed at PBLH over the desert area during daytime. This is a factor reducing PBLH of MOD_2 compared with MOD_1. Note that the area of minimum values in Fig. 15 occur where the maximum positive inclination of PBLH (Fig. 14). It is found that this area of maximum wind speed difference is located where there is maximum cool and moist bias of MOD_2 compared to MOD_1.

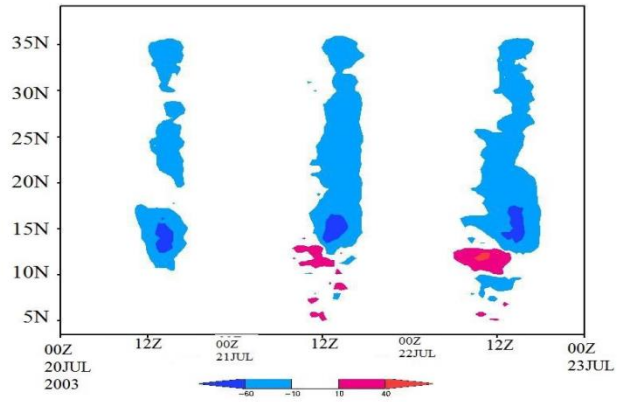

Figure 13. Same as Fig. 8 but for upward surface heat flux (wm^{-2}) difference $(MOD\_2 - MOD\_1)$.

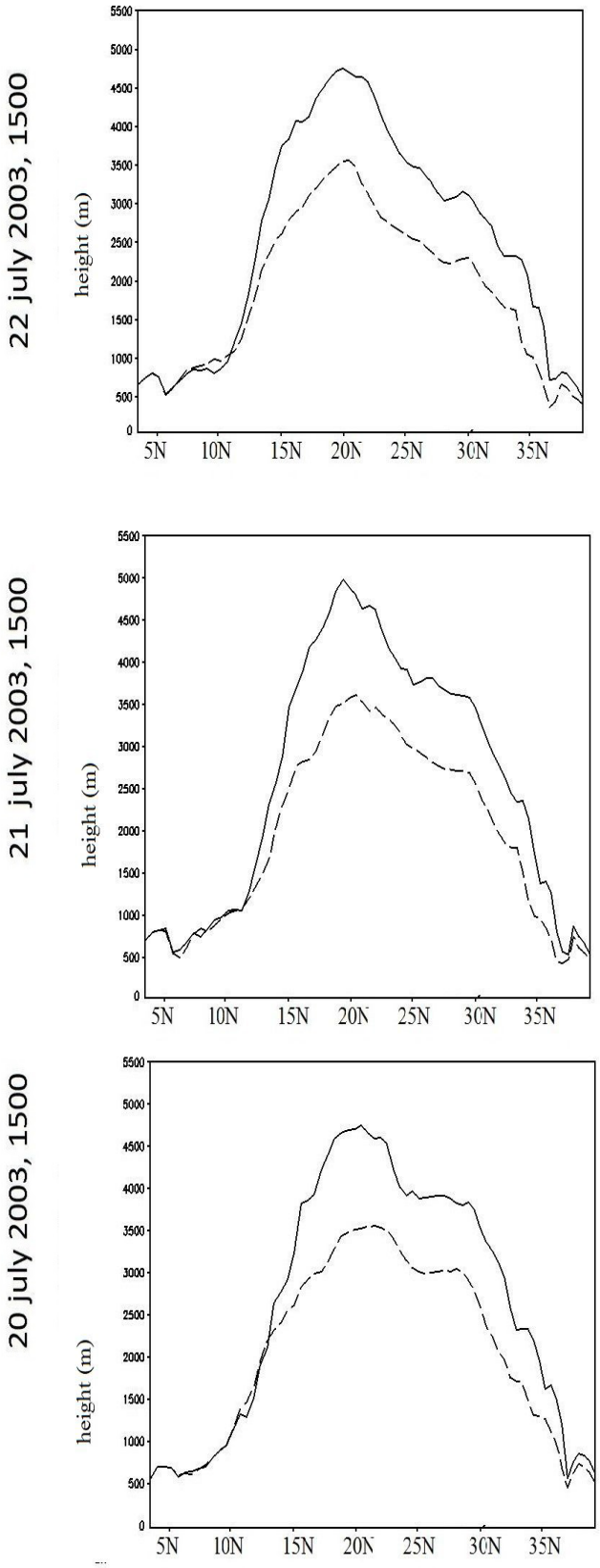

Figure 14. Same as Fig. 8 but for PBLH of MOD_1 (dashed line) and PBLH of MOD_2 (solid line).

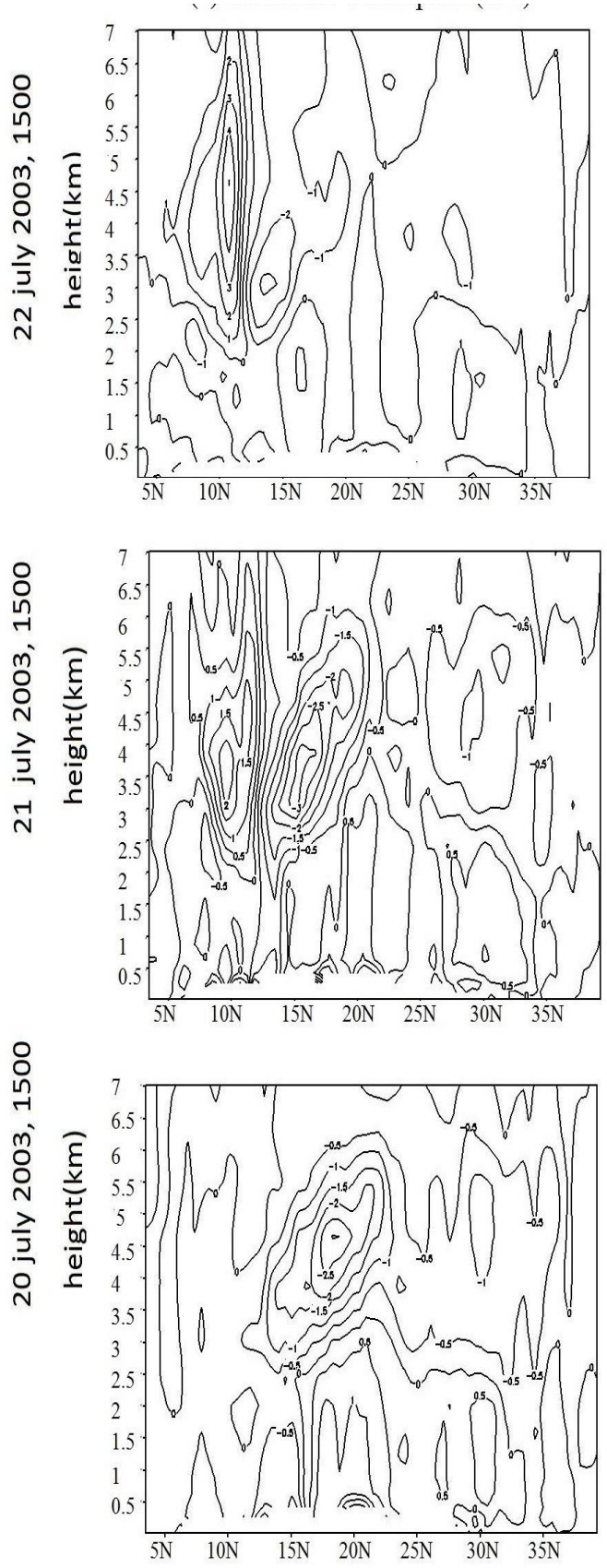

Figure 15. Same as Fig. 8 but for (a) horizontal wind speed difference $(MOD\_2 - MOD\_1)$ (m/s).

To summarize the above mentioned conclusions, Fig. 16 displays the models difference $(MOD\_2 - MOD\_1)$ of vertical distribution of potential temperature, water vapor mixing ratio and horizontal wind speed over the location $25^{\circ}N$; $25^{\circ}E$ at $15\,GMT$ on 20, 21 and 22 July 2003. The figure shows warm (cool) and dry (moist) bias of MOD_2 compared with MOD_1 in PBL (layer above PBL). This is typical distribution over the Sahara Desert (see also Fig. 8, 9, 10 and Fig. 11). On the other hand, Fig. 16 indicates that wind speed difference $(MOD\_2 - MOD\_1)$ has small negative values near the surface and minimum peak around PBLH. The minimum peak is found to be common feature over Sahara Desert during daytime. The mean wind speed in the lower PBL is found to be positive, i.e., MOD_2 has larger value as indicated by Fig. 15. Recently, Banks et al. (2016) show that the forecasted surface variables using WRF model tend to have a cool, moist and higher wind speed bias than observation. Our result seems to improve WRF model for both temperature and humidity but not for wind speed near the surface.

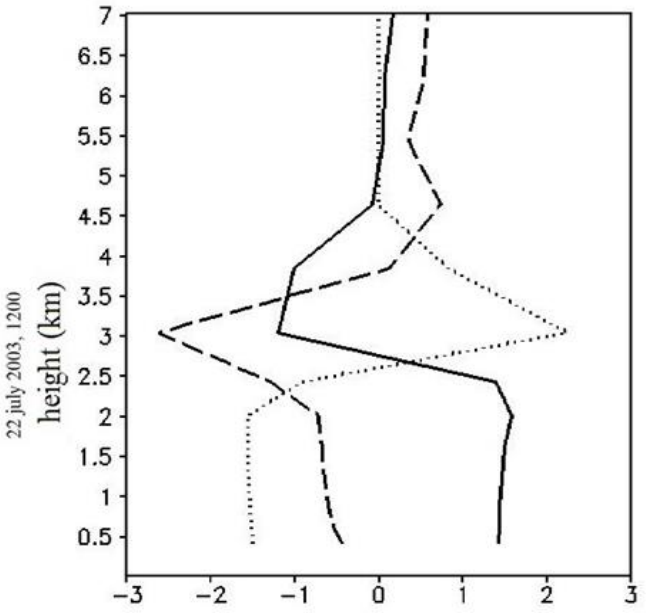

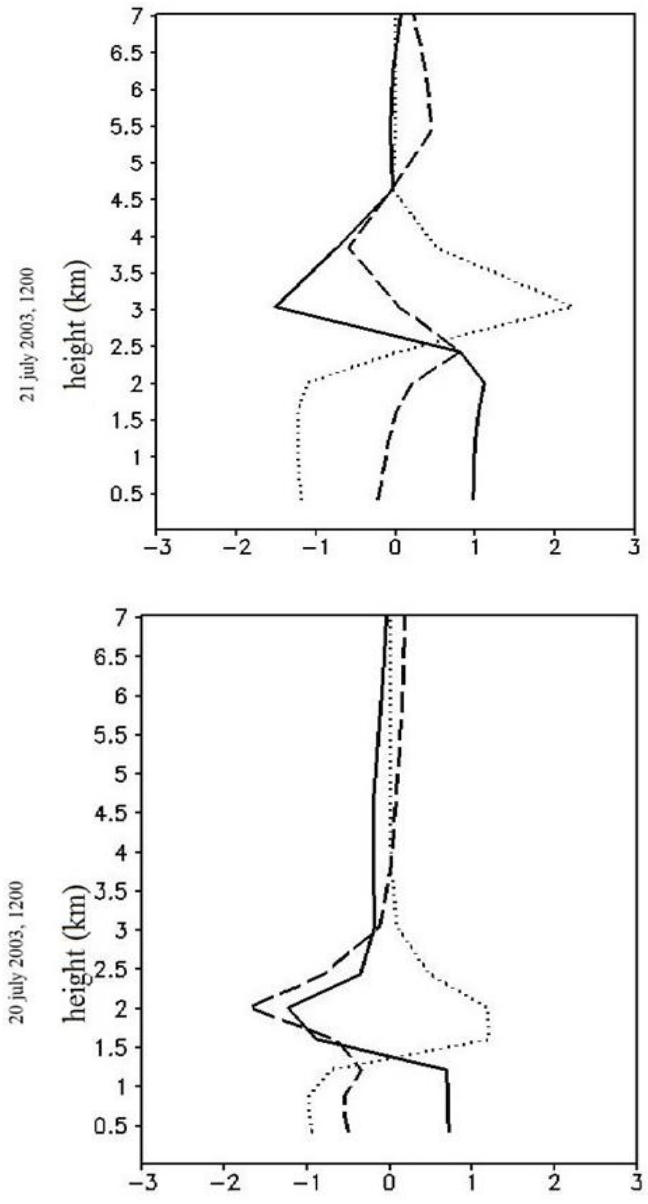

Figure 16. Vertical profile of the model deference $(MOD\_2a - MOD\_1)$ for potential temperature in $^{\circ}C$ (solid line); water vapor mixing ratio in g/kg (dotted line); wind speed in m/s (long dashed line).

D. Model result versus surface station observation

To show that MOD_2 output better simulates the atmospheric behavior compared with MOD_1, one needs observations such as radiosonds and Satellite data. Since such data is not available during the period of study with the required time resolution, surface weather station data are used. It comes out, as will be seen, that surface temperature and cloud development related to boundary layer can be used as indicators for the comparison. Follow comparison between two surface weather stations and the models output at the nearest grid point. The choice of a station is taken as the station is located in the Sahara Desert with no significant weather during the period 20-22 July 2003. The data is retrieved from the site "$https://www.underground.com$". It is found that for the three stations in Egypt (Cairo, Luxor and Aswan) where the sky is clear during the three days MOD_2 better simulates surface air temperature during the day. No low clouds or cloud related to PBL development are formed by the two models. In this section comparison between the models output and two surface weather stations in Niger are displayed. The two stations are Agadez ($17^{\circ}N;8^{\circ}E$) and Niamey ($13.5^{\circ}N;2.1^{\circ}E$). The nearest model grid point has the coordinates $17.2^{\circ}N;7.93^{\circ}E$ for Agadez and $13.44^{\circ}N;2.33^{\circ}E$ for Niamey. The data of Agadez station is only available from $0700\ AM$ to $0700\ PM$ local time (WAT) corresponding to $06\ AM$ to $06\ PM$ Coordinate Universal Time (UTC). The choice of these two stations is due to the fair weather they have during the three days as indicated in Tables 1 and 2. Both stations did not report any rain during the three days. One should keep in mind that the station data represents local scale while the grid point data represents regional scale $(0.5^{\circ} \times 0.5^{\circ})$. Comparison between grid point data and weather station data can be justified over topographically homogeneous area for weather element that has very weak gradient. For clear day, surface air temperature over most of the Sahara Desert regions can be such weather element. This is not the case for moisture or wind speed due to the local nature of these fields beside the urban effect where the surface weather station is located.

Figures 17 a,b,c show 2-meter air temperature, dew point, and 10-meter surface wind speed for MOD_1, MOD_2 and Agadez surface weather station for the three days 20, 21, and 22 July, 2003. One can note that the temperature of MOD_2 is closer to the station value and both are higher than MOD_1 except on the third day in late afternoon where the station temperature drops significantly (Fig. 17a). The station dew point temperature (Fig. 17b) indicates large drop of the dew point in the afternoon that is also indicated by MOD_1 and MOD_2. It is not clear which model better simulates the station data. The figure also indicates that on the first day the model moisture is very low compared with the actual value. For surface wind speed, 10 meters above surface, Fig. 17c suggests better simulation of

MOD_1 on 20 July while MOD_2 wind speed values are closer to the station data on 21 and 22, July 2003. PBLH and the vertical distribution of cloud fraction for MOD_1 and MOD_2 are displayed in Figs. 18a,b,c. As expected PBLH of MOD_2 have larger values than MOD_1 in early afternoon that drops significantly to be less than MOD_1 in late afternoon (Fig. 18a). One can note that there is no cloud formation associated with PBL development for MOD_1 (Fig. 18b). On the other hand, cloud formation associated with PBL development is clear for MOD_2 that started in early afternoon on 21, and 22 July 2003 (Fig. 18c). The lack of similar cloud on 20 July seems related to the low model moisture on that day as mentioned above (Fig. 17b). The sky condition for Agadez station shown in Table 1 indicates no cloud in the morning and clouds in the afternoon supporting MOD_2 simulation. It is found that the formation of cloud that is formed above PBL starts after PBLH reaches its maximum value, i.e., has base height less than the maximum PBLH. Vertical velocity difference ($MOD\_2 - MOD\_1$) which is shown in Fig. 18c indicates the development of strong upward motion that accompany the cloud formation of MOD_2.

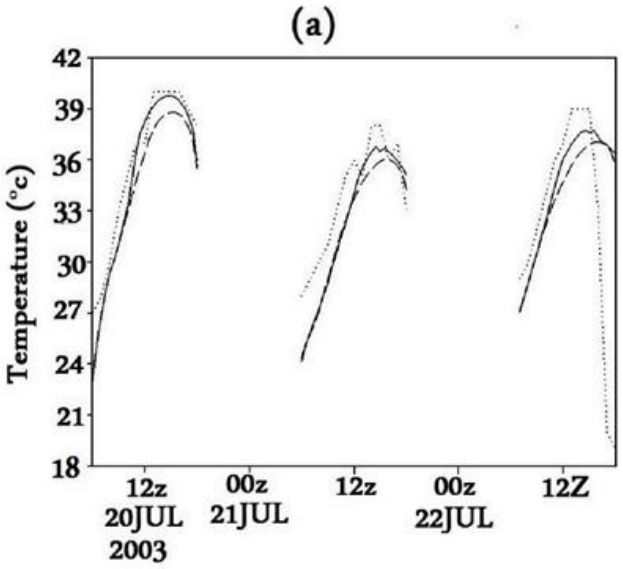

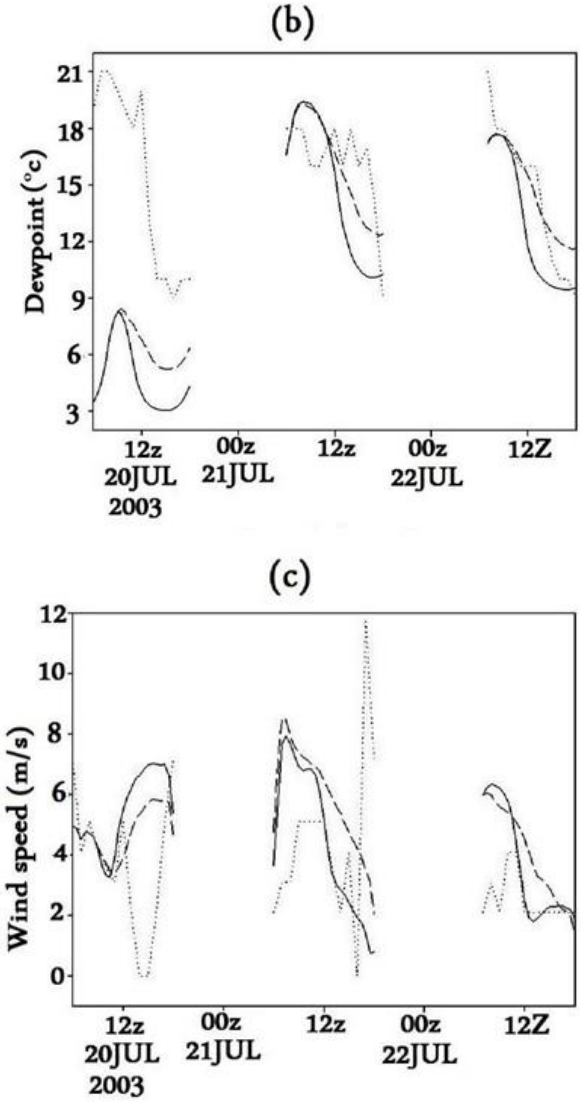

Figure 17. (a) Surface air temperature in $^{\circ}C$; (b) Surface dew point temperature in $^{\circ}C$; (c) wind speed in m/s.

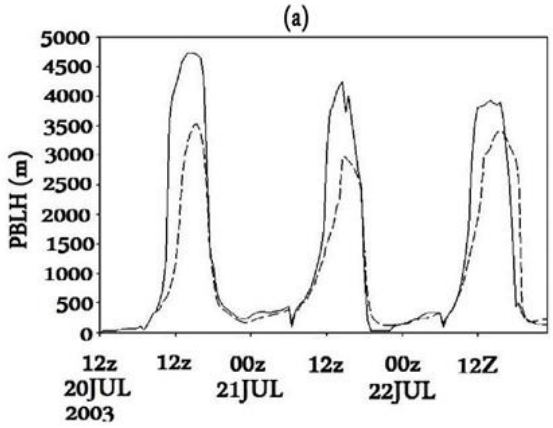

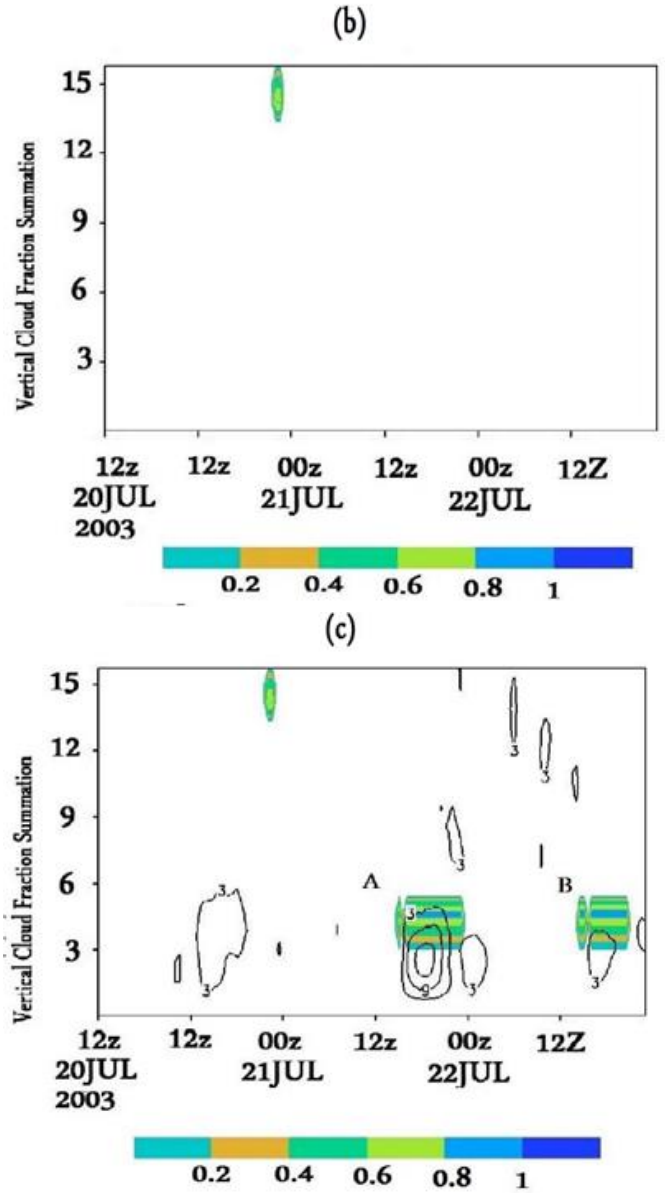

Figure 18. (a) PBLH in m; (b) Cloud fraction (MOD_1); (c) Cloud fraction (MOD_2) and vertical wind speed difference $(MOD\_2 - MOD\_1)$ in m/s. MOD_1 dashed line; MOD_2 solid line; Agadez surface weather station dotted line.

Table 1. Sky condition for Agadez on July 20, 21, and 22, 2003

TIME(UTC)	20 July 2003	21 July 2003	22 July 2003
12:00 AM	———	———	———
1:00 AM	———	———	———
2:00 AM	———	———	———
3:00 AM	———	———	———
4:00 AM	———	———	———
5:00 AM	———	———	———
6:00 AM	Clear	Clear	———
7:00 AM	Clear	Clear	Mostly Cloudy
8:00 AM	Clear	Clear	Clear
9:00 AM	Clear	Clear	Clear
10:00 AM	Clear	Clear	Clear
11:00 AM	Clear	Clear	Clear
12:00 PM	Clear	Mostly Cloudy	Clear
1:00 PM	Mostly Cloudy	Mostly Cloudy	Scattered Clouds
2:00 PM	Mostly Cloudy	Mostly Cloudy	Clear
3:00 PM	Scattered Clouds	Partly Cloudy	Scattered Clouds
4:00 PM	Mostly Cloudy	Partly Cloudy	Clear
5:00 PM	Mostly Cloudy	Unknown	Unknown
6:00 PM	Clear	Unknown	Clear
7:00 PM	———	———	———
8:00 PM	———	———	———
9:00 PM	———	———	———
10:00 PM	———	———	———
11:00 PM	———	———	———

Figure 19 and 20 is similar to Fig. 17 and 18 respectively but for Niamey surface weather station. One can note a large difference between model air temperature and Niamey surface weather station on the first day (Fig. 19a). This difference can be associated with the cloudy sky as indicated in Table 2. In such case local value cannot be compared with the model value. Also the model accuracy to predict cloud fraction is generally not high. On the second and third days the difference is reduced with MOD_1 being closer to the surface station (Fig 19a). The station dew point temperature (Fig. 19b) shows large difference with MOD_1 and MOD_2. On the other hand, surface wind speed (Fig. 19c) for MOD_2 has mean value closer to the station data for the three days. Figs. 20a,b,c show PBLH and cloud fraction for MOD_1 and MOD_2. Again, as expected PBLH of MOD_2 is higher than MOD_1 in

early afternoon then drops significantly in late afternoon to be less than that of MOD_1 (Fig. 20a). There is clouds development by both models with MOD_2 being more cloudy (Figs. 20b,c). All clouds Formed in MOD_1 are there in MOD_2. What is interesting is the clouds marked A and B in Fig. 20c. These clouds are directly correlated to PBL development as they are formed in late afternoon with base height less than the maximum PBLH. Note that in the third day no clouds are formed in MOD_1 (Fig. 20b) while Table 1 shows cloudy day. On day two MOD_2 does not show cloud related to PBL development since there are clouds above PBL (Fig. 20c). Vertical velocity difference ($MOD\_2 - MOD\_1$) which is shown in Fig. 20c shows strong upward motion that accompany clouds correlated with PBL development.

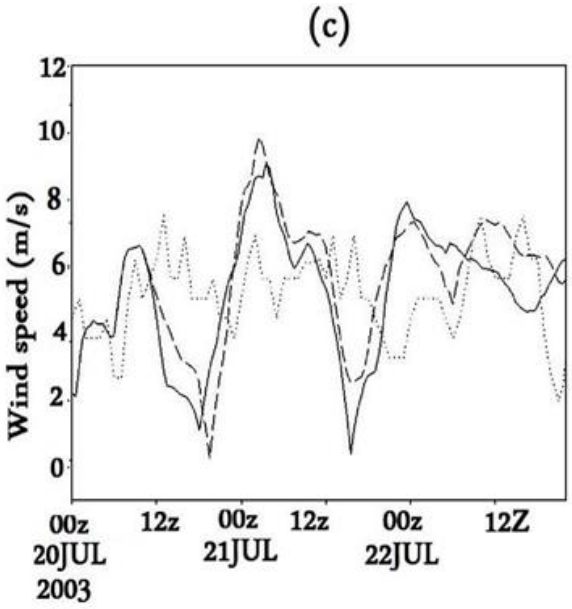

Figure 19. Same as Fig. 17 but for Niamey surface weather station.

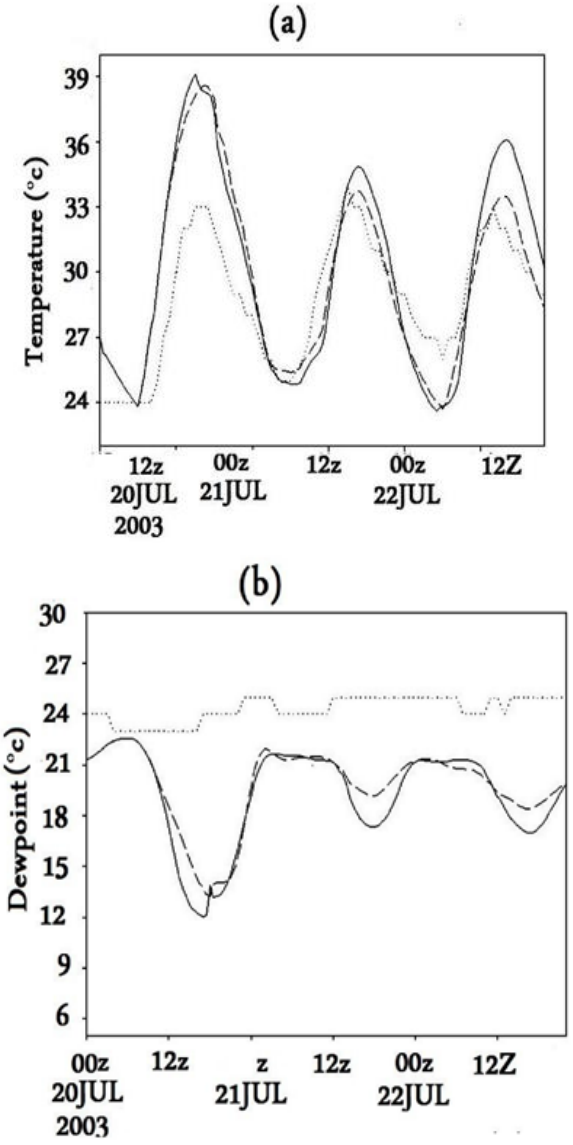

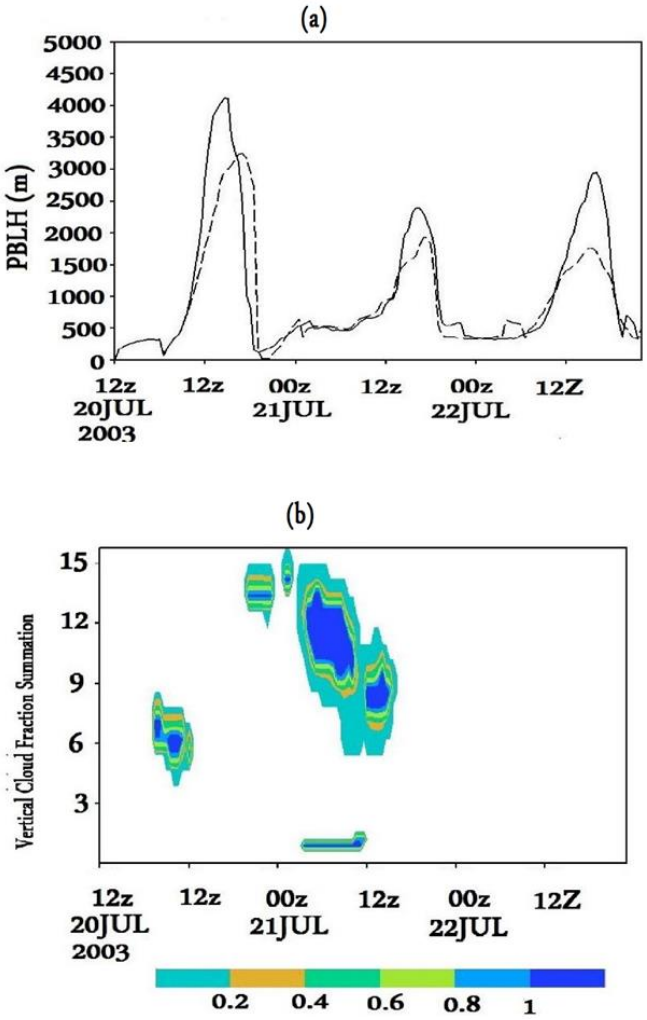

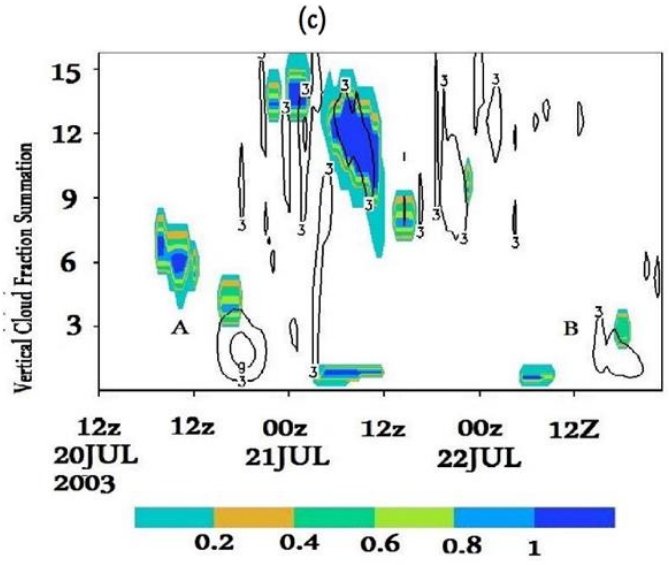

Figure 20. Same as Fig. 18 but for Niamey surface weather station.

Table 2. Sky condition for Miamey on July 20, 21, and 22, 2003

TIME(UTC)	20 July 2003	21 July 2003	22 July 2003
12:00 AM	Clear	Clear	Clear
1:00 AM	Mostly Cloudy	Clear	Clear
2:00 AM	Mostly Cloudy	Clear	Clear
3:00 AM	Mostly Cloudy	Clear	Clear
4:00 AM	Mostly Cloudy	Clear	Clear
5:00 AM	Mostly Cloudy	Clear	Clear
6:00 AM	Mostly Cloudy	Clear	Clear
7:00 AM	Mostly Cloudy	Clear	Mostly Cloudy
8:00 AM	Clear	Scattered Clouds	Mostly Cloudy
9:00 AM	Clear	Scattered Clouds	Mostly Cloudy
10:00 AM	Clear	Mostly Cloudy	Clear
11:00 AM	Clear	Mostly Cloudy	Scattered Clouds
12:00 PM	Clear	Mostly Cloudy	Scattered Clouds
1:00 PM	Clear	Mostly Cloudy	Scattered Clouds
2:00 PM	Clear	Mostly Cloudy	Scattered Clouds
3:00 PM	Clear	Mostly Cloudy	Scattered Clouds
4:00 PM	Mostly Cloudy	Mostly cloudy	Mostly Cloudy
5:00 PM	Mostly Cloudy	Mostly Cloudy	Scattered Clouds
6:00 PM	Mostly Cloudy	Mostly Cloudy	Scattered Clouds
7:00 PM	Mostly Cloudy	Mostly Cloudy	Scattered Clouds
8:00 PM	Mostly Cloudy	Mostly Cloudy	Scattered Clouds
9:00 PM	Clear	Mostly Cloudy	Clear
10:00 PM	Clear	Mostly Cloudy	Scattered Clouds
11:00 PM	Clear	Clear	Clear

To summarize, for clear and fair weather, MOD_2 better simulates surface air temperature during the day as well as clouds related to PBL development. Although more evidence is needed to support the above discussion but as mentioned earlier, (Banks et~al.(2015)Banks, Tiana-Alsina, Rocadenbosch,, and Baldasano) and (Banks et~al.(2016)Banks, Tiana-Alsina, Baldasano, Rocadenbosch, Papayannis, Solomos,, and Tzanis) support our results for PBLH, surface temperature, and moisture. As quoted by (Banks et~al.(2015)Banks, Tiana-Alsina, Rocadenbosch,, and Baldasano) “Overall, there is a systematic underestimation of PBL height simulated in the WRF model". (Banks et~al.(2016)Banks, Tiana-Alsina, Baldasano, Rocadenbosch, Papayannis, Solomos,, and Tzanis) in their conclusion mention “The largest differences between model and observations are found with simulated PBL height during Saharan synoptic flows. During the daytime, campaign-averaged near-surface variables show WRF tended to have a cool, moist bias with higher simulated wind speeds than the observations, especially near the coast".

E. Unexpected forecast feature

As mentioned above, to simulate observation of PBLH over the desert area during the daytime an increase in θ_s is performed to represents surface layer temperature. One expects, by this modification, that PBLH of MOD_1 will never exceeds that of MOD_2. It is found in the last section that MOD_2 has higher amount of clouds which cause in late afternoon areas with PBLH significantly less than MOD_1. On the other hand, it is found that there

are many local areas south of the Sahara Desert where PBLH of MOD_1 differs significantly from that of MOD_2. To understand the cause of these differences, several model runs (MOD_2a) are performed where the modification of θ_s is carried out over limited area and for limited period of time.

The first experiment of MOD_2a, θ_s is permitted to increases when the skin temperature $\hat{a}$ is over $40^{\circ}C$ by the amount $(TSK-40)/3.5$ only over the area around the grid point $30^{\circ}E$; $20^{\circ}N$ (36 grid points; 6 grid points in both x and y directions). The start time of activation is $7:35\,GMT$ up to $8:00\,GMT$, i.e., for successive six time steps. Figure 21a shows two meters surface temperate field difference (MOD_2a - MOD_1) at $8:00\,GMT$, i.e., half an hour after the onset of the thermal activation. Figure 21b shows the vorticity field for the wind field difference (MOD_2a - MOD_1) at $8:00\,GMT$. Figure 21b shows the formation of a dipole vortex and the propagation of fast small scale disturbances out of the activated area. The figure indicates that the disturbance propagates more than 10° in half an hour, i.e., with very high speed. These waves, which are of small scale type, propagate in both horizontal and vertical directions. One expects that horizontal and vertical short waves for both sound and gravity are exited due to the thermal forcing applied. The figure also indicates that the field of disturbance is nearly isotropic. Miller (2002) shows that for short waves where $k > N/C$ the dispersion equation for the linearized atmospheric basic equations in x-z plane reduces to the form:

$$\omega_g = \pm \frac{Nk}{\sqrt{k^2+m^2+\frac{1}{4H_0^2}}},\ and\ \omega_a = \pm C\sqrt{k^2+m^2+\frac{1}{4H_0^2}}, \tag{5}$$

where k and m are the wave numbers in x and z directions respectively, H_0 is the atmospheric scale height, N is the Brunt $Väisälä$ frequency, C is the speed of sound, ω_g and ω_a are the frequencies of gravity and sound waves respectively. The phase and group velocities obtained from (5) are less than that indicated by Fig. 21a One can anticipate that the dispersion equation of the finite difference equation that is also function of Δt, Δx, Δy and Δz is necessary to explain this fast propagation. Fig. 21c shows the divergence for the wind field difference of $(MOD\_2a - MOD\_1)$ on June, 20 at $11:00\,GMT$, i.e., three hours after activation. One notes, on several locations, the development of dipole vorticies and the propagation of gravity wave through geostrophic adjustment (Snyder et al. 2007). The development occurs after the small fast disturbances hit these locations. It is known that topography, convection, and wind shear are among the sources of atmospheric gravity waves excitation (Fritts and Alexander 2003). It is found that X_1 and X_2, that are marked in Fig. 21c are locations with deep convection. The local development that occurs at the mentioned locations led to significant local differences between MOD_2a and MOD_1. For example after one day forecast the temperature (PBLH) difference between the two models at local areas south of $15^{\circ}N$ have values between $-5^{\circ}C$ and $4^{\circ}C$ ($-1500\ m$ and $1500\ m$) which is significant.

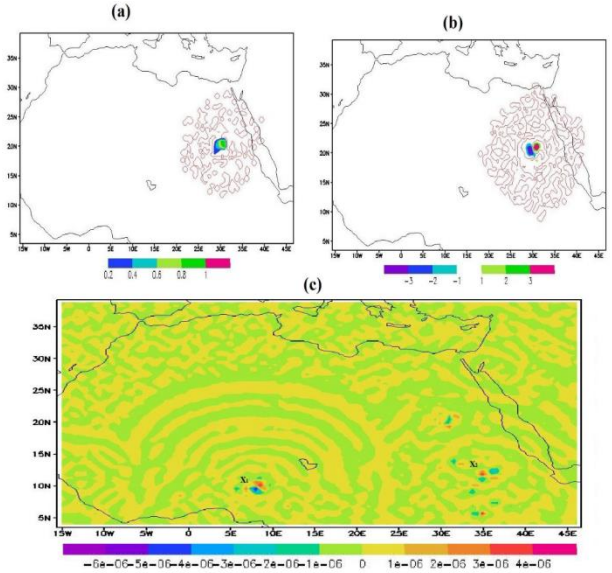

Figure 21. (a) two meters temperature difference ($^{\circ}C$) $(MOD\_2a - MOD\_1)$ on 20 July 2003 at 08:00 GMT. (b) same as (a) but for voticity of wind vector difference $(10^6 sec^{-1})$. (c) the divergence of the wind vector difference (sec^{-1}) $(MOD\_2a - MOD\_1)$ on 20 July 2003 at 11:00 GMT.

Other experiments where θ_s is increased by $0.2^{\circ}C, 0.5^{\circ}C, 1.0^{\circ}C$, and $5.0^{\circ}C$ only once at only one specific location ($20.9^{\circ}N$; $15^{\circ}E$) are performed. The impacts of these forcing on the model outputs are

compared. It is found, for these experiments, that the overall mean features are not significantly different. That is to say the same scenario is repeated and that the overall output features for the four experiments are similar. In fact it is found that developments occur at the same locations for the four experiments and that the magnitude of development is not function of the initial forcing. It is also concluded that the fast disturbances have very small magnitude, at least one order of magnitude less than the change that occur due to development.

IV. CONCLUSION

It is found that the Weather Research and Forecasting (WRF) model version 3.6.1 implemented with Yonsei University (YSU) Planetary Boundary Layer (PBL) scheme, underestimates significantly Planetary Boundary Layer Height (PBLH) over the Sahara Desert in summer months during daytime. It is anticipated that the estimated scheme temperature near the surface that should resembles the surface layer temperature is not appropriate. In this work a revised version of YSU PBL scheme is developed where the temperature near the surface θ_s is raised by $(TSK-40)/d$ only when the skin temperature (TSK) is higher than $40^{\circ}C$. It is shown that the optimal value of the parameter d is 3.5. The result of forecasting the situation 20 July 2003 for three days using WRF model implemented with the new version of YSU scheme is presented in this work. The results show that the model estimation of PBLH approach values anticipated from the two data sets ECMWF ERA-Interim reanalysis data and NCEP reanalysis data. Also comparison, over the Sahara Desert where the thermal forcing is applied, between WRF model output runs with the modified PBL YSU scheme MOD_2 and runs with PBL YSU not modified MOD_1 gives:

1- Higher (lower) values of temperature in PBL (layer above PBL) for MOD_2 compared with MOD_1.

2- Lower (higher) values of water vapor mixing ratio in PBL (layer above PBL) for MOD_2 compared with MOD_1.

3- Lower values of wind speed in PBL with peak around PBLH for MOD_2 compared with MOD_1.

4- Higher values of cloud fraction for MOD_2 compared with MOD_1.

Recently, Banks et al. (2016) show that WRF model tended to have cool, moist bias near the surface. Our results seems to improve WRF model in these respects. On the other hand, they mentioned, contrary to our result, that WRF model has higher surface wind speed than observation. To assure that MOD_2 output better simulates observations compared with MOD_1, observation data such as Satellite, and Radiosonds data are needed. These data are not available over the Sahara Desert during the period of study with adequate time resolution. It is found that the surface weather stations data can be used to compare surface air temperature and clouds related to PBL development. Comparison between surface weather station observations and model output at grid points, that has different resolutions, can be justified for air surface temperature since this field has weak gradient over Sahara Desert. Comparison among MOD_1, MOD_2, and quite a few surface weather stations located in Sahara Desert show that:

1- MOD_2 better simulates air surface temperature on clear and fair weather during daytime.

2- MOD_2 better simulates clouds related to PBL development.

The impact on the WRF model output due to applying the thermal forcing over limited area and a few time steps is also studied. It is shown that once the forcing is activated a local dipole vortex is formed accompanied with the propagation of very small fast disturbances. As these disturbances reach certain locations local dipole vortices are developed that act as sources of gravity wave propagation. It is shown that cloud convection regions are among areas that are vulnerable for development by these very small fast disturbances. The development that occurs on local scale causes significant change on weather elements. One can note that this significant impact occurs far away from the activated source, and thus resembles the Butterfly effect. One can argue that since very small disturbances are part of the real chaotic atmosphere, the development that is caused by a far source and symbolize the Butterfly effect is a numerical rather than a physical outcome.

V. REFERENCES

[1]. Ao, Waliser, Chan, Li, Tian, Xie,, and Mannucci) Ao, C. O., D. E. Waliser, S. K. Chan, J.-L. Li, B. Tian, F. Xie, and A. J. Mannucci, 2012: Planetary boundary layer heights from gps radio occultation refractivity and humidity profiles. J. Geophys. Res., 117, D16 117, doi:10.1029/2012JD017598 .

[2]. Banks, R. F., J. Tiana-Alsina, J. M. Baldasano, F. Rocadenbosch, A. Papayannis, S. Solomos, and C. G. Tzanis, 2016: Sensitivity of boundary-layer variables to pbl schemes in the wrf model based on surface meteorological observations, lidar, and radiosondes during the hygra-cd campaign. J. Atmospheric Research, 176-177, 185–201, doi:org/10.1016/j.atmosres. 2016.02.024.

[3]. Banks, R. F., J. Tiana-Alsina, F. Rocadenbosch, and J. M. Baldasano, 2015: Performance evaluation of the boundary-layer height from lidar and the weather research and forecasting model at an urban coastal site in the north-east Iberian peninsula. Boundary-Layer Meteorol, 157, 265–292, doi:10.1007/s10546-015-0056-2.

[4]. Bao, J. W., S. A. Michelson, P. O. G. Persson, I. V. Djalalova, and J. M. Wilczak, 2008: Observed and wrf-simulated low-level winds in a high-ozone episode during the central california ozone study. J. Appl. Meteorol. Climatol, 47, 2372–2394, doi:10.1175/2008jamc1822.1.

[5]. Cheng, F. Y., S. C. Chin, and T. Liu, 2012: The role of boundary layer schemes in meteorological and air quality simulations of the taiwan area. Atmos. Environ., 54, 714–727, doi:10.1016/j.atmosenv.2012.01.029.

[6]. Dee, D. P., and Coauthors, 2011: The era-interim reanalysis: Configuration and performance of the data assimilation system. Q. J. R. Meteorol. Soc., 137, 553â€“597, doi:10.1002/qj.828.

[7]. Fritts, and Alexander) Fritts, D. C., and M. J. Alexander, 2003: Gravity wave dynamics and effects in the middle atmosphere. Rev. Geophys., 41(1), 1003, doi:10.1029/2001RG000106.

[8]. Garcia-Diez, M., J. Fernndez, L. Fita, and C. Yage, 2013: Seasonal dependence of wrf model biases and sensitivity to pbl schemes over europe. Quart. J. Roy. Meteorol. Soc., 139, 501–514.

[9]. Garcia-Menendez, F., Y. Hu, and M. T. Odman, 2013: Simulating smoke transport from wildland fires with a regional-scale air quality model sensitivity to uncertain wind fields. Geophys Res. Atmos., 118, 6493–6504, doi:10.1002/ jgrd.50524.

[10]. Gilliam, R. C., J. Godowitch, and S. T. Rao, 2012: Improving the horizontal transport in the lower troposphere with four dimensional data assimilation. Atmos. Environ., 53, 186–201, doi:10.1016/j.atmosenv.2011.10.064.

[11]. Hong, S. Y., Y. Noh, and J. Dudhia, 2006: A new vertical diffusion package with an explicit treatment of entrainment processes. Mon. Wea. Rev., 134(9), 2318–2341, doi:10.1175/Mwr3199.1.

[12]. Ibrahim, M. M., M. Abdel-Sattar, and A.-R. M. Lasheen, 2012: Comparison among three planetary boundary layer schemes in the wrf model. Al-Azhar Bull Sci., 23, 39–49.

[13]. Jin, M., and R. E. Dickinson, 2010: Land surface skin temperature climatology: benefitting from the strengths of satellite observations. Environ. Res. Lett., 5, 044 004, doi:10.1088/1748-9326/5/4/044004.

[14]. Miller, M., 2002: Atmospheric waves. meteorological training course lecture series. ECMWF, pp.200.

[15]. Richardson, H., S. Basu, and A. A. M. Holtslag, 2013: Improving stable boundary-layer height estimation using a stability-dependent critical bulk richardson number. Bound.-Lay. Meteorol, 148, 93–109, doi:10.1007/s10546-013-9812-3.

[16]. Snyder, C., D. J. Muraki, R. Plougonven, and F. Zhang, 2007: Inertia gravity waves generated within a dipole vortex. Atmos. Sci., 64, 4417–4431, doi:10.1029/JC091iC11p12865.

[17]. Sugiyama, G., and J. S. Nasstrom, 1999: Methods for determining the height of the atmospheric boundary layer. LLNL Report UCRL-ID-133200, LLNL.

[18]. von Engeln, and Teixeira) von Engeln, A., and J. Teixeira, 2013: A planetary boundary layer height climatology derived from ecmwf re-analysis data. Journal of Climate, 26, 6575–6590, doi:10.1175/JCLI-D-12-00385.1.

[19]. Zhang, Y., Z. Gao, D. Li, Y. Li, N. Zhang, X. Zhao, and J. Chen, 2014: On the computation of planetary boundary-layer height using the bulk richardson number method. Geosci. Model Dev., 7, 2599–2611.